materials

MDPI

Article

Synergetic Effect and Phase Engineering by Formation of $Ti_3C_2T_x$ Modified 2H/1T-$MoSe_2$ Composites for Enhanced HER

Lei Xiao [1], Qichao Yang [2], Xiangyang Zhu [2], Yang Wei [3,*] and Jing Wang [1,*]

[1] School of Integrated Circuits, Tsinghua University, Beijing 100084, China; xiaolei@mail.tsinghua.edu.cn
[2] School of Materials Science and Engineering, University of Science and Technology Beijing, Beijing 100083, China; 18866986789@163.com (Q.Y.); 202310192378@mail.scut.edu.cn (X.Z.)
[3] Department of Physics and Tsinghua-Foxconn Nanotechnology Research Center, Tsinghua University, Beijing 100084, China
* Correspondence: weiyang@tsinghua.edu.cn (Y.W.); wang_j@mail.tsinghua.edu.cn (J.W.)

Abstract: The typical semi conductivity and few active sites of hydrogen evolution of 2H $MoSe_2$ severely restrict its electrocatalytic hydrogen evolution performance. At the same time, the 1T $MoSe_2$ has metal conductivity and plentiful hydrogen evolution sites, making it feasible to optimize the electrocatalytic hydrogen evolution behavior of $MoSe_2$ using phase engineering. In this study, we, through a simple one-step hydrothermal method, composed 1T/2H $MoSe_2$, and then used newly emerging transition metal carbides with several atomic-layer thicknesses $Ti_3C_2T_x$ to improve the conductivity of a $MoSe_2$-based electrocatalyst. Finally, $MoSe_2$@$Ti_3C_2T_x$ was successfully synthesized, according to the control of the additional amount of $Ti_3C_2T_x$, to form a proper $MoSe_2$/$Ti_3C_2T_x$ heterostructure with a better electrochemical HER performance. As obtained $MoSe_2$@4 mg-$Ti_3C_2T_x$ achieved a low overpotential, a small Tafel slope and this work offers additional insight into broadened $MoSe_2$ and MXenes-based catalyst's electrochemical application.

Keywords: $MoSe_2$@$Ti_3C_2T_x$ heterostructures; hydrogen evolution reaction; phase structure

Citation: Xiao, L.; Yang, Q.; Zhu, X.; Wei, Y.; Wang, J. Synergetic Effect and Phase Engineering by Formation of $Ti_3C_2T_x$ Modified 2H/1T-$MoSe_2$ Composites for Enhanced HER. *Materials* **2023**, *16*, 6991. https://doi.org/10.3390/ma16216991

Academic Editors: Natalia I. Tsyntsaru and Henrikas Cesiulis

Received: 26 September 2023
Revised: 26 October 2023
Accepted: 27 October 2023
Published: 31 October 2023

1. Introduction

Hydrogen energy is one of the most prevalent potential candidates for renewable clean energy with high energy capacity to replace fossil fuel [1–3]. However, up to now, the most used industrial hydrogen production is still electrochemical water splitting [4–6]. Electrochemical HER is a cathode double-electron-transfer reaction that begins with the Volmer step, in which electrons are transferred to the cathode surface, bind to H+ at an unoccupied active site, and produce adsorbed H*. Currently, noble metals are the most feasible catalysts for electrochemical water splitting to reduce overpotential and simultaneously facilitate reaction kinetics of hydrogen evolution reaction (HER) [7–9]. Their scarcity and high price significantly restrict further commercial development and large-scale applications of these noble metals for water-splitting. Hence, finding cheap and earth-abundant electrocatalytic electrodes is essential to accelerating the commercial application of hydrogen energy.

Two-dimensional transition-metal dichalcogenides (2D TMDs) have many promoting properties for HER; 2D TMD's atomically thin-based structure increased reaction surface area and available active site [10], and different transition metals have various d orbitals. Thus, exhibiting different catalytic performance makes it feasible to improve the HER performance by doping different metal elements [11,12]. However, excellent catalytic activity and low cost compared to noble metals give it considerable potential in HER. $MoSe_2$, as a member of the 2D transition-metal dichalcogenide (TMDC), has received widespread attention due to its corrosion stability [13], chemically tunable electronic properties [14–18]. $MoSe_2$ can present as a octahedral coordination 1T (tetragonal symmetry, one layer per repeat unit, octahedral coordination) phase with metallic properties and a triangular

coordination 2H (hexagonal symmetry, two lavers per repeat unit, trigonal prismatic coordination) phase with semiconductor properties. However, $MoSe_2$ electrochemical HER performances mainly depend upon its nanostructure and Crystalline phase, but for 2H phase $MoSe_2$, lack of active sites and weak conductivity restrict its performance in electrochemical HER [19–21]. Researchers use commonly used regulatory methods to improve their electrochemical performance such as strain engineering [22], surface/interface engineering [23], alloy engineering [24,25], defect engineering [26], and compounds with other materials [27–30]. However, designing and fabricating excellent $MoSe_2$-based composite catalysts for HER is of great fundamental importance to promoting TMDC-catalyst use of clean energy.

In this study, we, through a simple one-step hydrothermal method, use an emerging type of 2D transition-metal carbide $Ti_3C_2T_x$ (T = -F, -OH, -O terminal group) to improve the conductivity of $MoSe_2$-based electrocatalysts, $Ti_3C_2T_x$. A typical MXene material is a typically a layered material with a sandwich structure consisting of three alternating layers of Ti atoms and two alternating layers of C atoms. In addition, due to the introduction of a small number of residual chemical elements during the preparation process of acid-solution etching, the surface adsorbs rich terminal groups such as -F, -OH, -O, etc. As a conductor can improve the HER performance of $MoSe_2$ [31], the addition amount of $Ti_3C_2T_x$ must be controlled accordingly to form a proper $MoSe_2/Ti_3C_2T_x$ heterostructure which has a better electrochemical HER performance. A small Tafel slope (79 mV dec^{-1}) and low overpotential (−185.29 mV) were achieved with the obtained $MoSe_2$@4 mg-$Ti_3C_2T_x$. However, the $Ti_3C_2T_x$ improves the performance of 1H/2H nanoflower-like $MoSe_2$ in HER and is still not researched. This work utilizes $Ti_3C_2T_x$ as a composite substrate, and controls the $MoSe_2$ two-phase ratio. Both of these simultaneously enhance catalytic activity, which has significance for applying TMDC materials in the HER catalytic field.

2. Experiment Section

2.1. Synthesis of $Ti_3C_2T_x$ MXene Nanosheets

Firstly, via a relatively safe method, we combined a 5 wt % LiF powder and a 1 mol/HCl solution-etching in a glove box inert atmosphere, using a magnetic force-driving stirred reactor for the reaction. After heating in an oil bath for 96 h, AlF_3 is generated from the bulk-layered MXene phase, and Ti_3AlC_2 raw material is used to remove Al and generate $Ti_3C_2T_x$. Then, ultrasonic dispersion and cleaning are carried out to obtain the required few-layer $Ti_3C_2T_x$ thin sheets. The material was then dried in a vacuum-drying oven for 12 h. The product was then ground into powder in an agate mortar, collected, and vacuumed, successfully preparing layered $Ti_3C_2T_x$.

2.2. Carbon Cloth Preprocess for Hydrophilic Treatment

According to the volume ratio of 4:1, we mixed 10% HNO_3 and 20% H_2SO_4; soaked the carbon cloth (1 cm × 1 cm) at room temperature for 12 h; took it out, and put it in ultrasonic ethanol solution for 30 min; then, used DI water wash for 30 s; and repeated 3 times to remove the residual acid. It must be sealed and stored in deionized water.

2.3. Preparation of 1T/2H Phase $MoSe_2$@$Ti_3C_2T_x$ on CC

Figure 1 shows that Se powder (1.0 mmol) was dissolved into 15% hydrazine hydrate. Magnetic solution was stirred and kept for 24 h. At the same time, a few $Ti_3C_2T_x$ powders were dispersed with ultrasound (600 W) in 20 mL deionized water for 30 min; then, 1 mmol of $Na_2MoO_4 \cdot 2H_2O$ was added to the dispersion and stirred for 45 min. After that, we added the reduced Se ion solution to the dispersion and sealed it in a 50 mL high-pressure reactor, using a carbon cloth (1 cm × 1 cm) as the loaded substrate, and then heated it to 180 °C for insulation for 24 h. After cooling, the sample was washed and dried in a vacuum environment of 60 °C. During the process, attention should be paid to preventing oxidation.

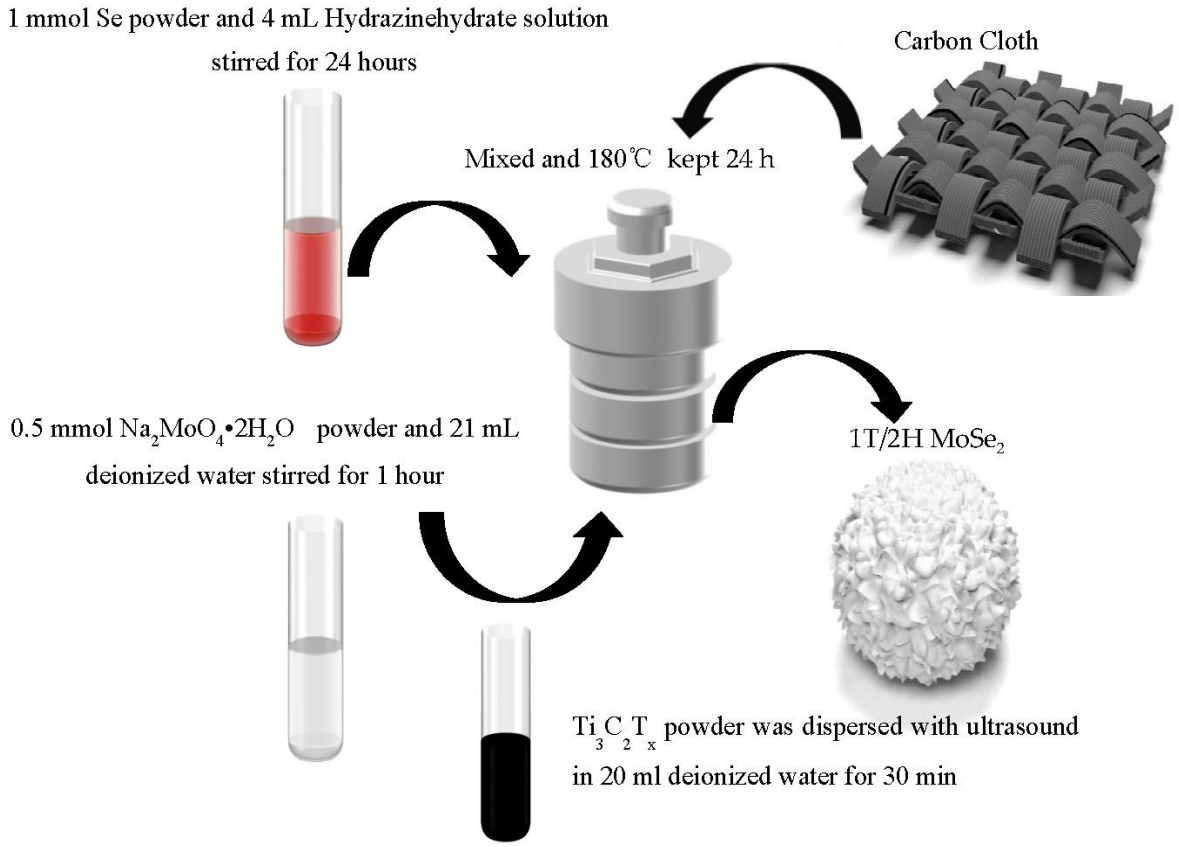

Figure 1. Schematic diagram of hydrothermal preparation of 1T/2H $MoSe_2$@$Ti_3C_2T_x$.

2.4. Characterization

The morphology of the sample was characterized using field emission scanning electron microscopy (FEI, HONG KONG, SEM, FEI Nova 400), and X-ray diffraction (XRD) patterns were recorded using Cu Ka radiation on Rigaku D/Max 4000 V to determine sample-composition information. Raman spectral information was obtained using a confocal microscope (HORIBA FRANCE LabRAM HR Evolution), using a 532 nm laser at low power. XPS (Thermo ESCALAB 250XI) determined the chemical configuration.

2.5. Electrochemical Measurement

The electrocatalytic HER measurement of the obtained products was conducted using a standard three-electrode electrochemical workstation consisting of an electrode counter electrode (Pt), a reference electrode Ag/AgCl, and a stainless-steel working electrode. All the electrocatalytic HER measurements were performed in 1 mol/L H^+ solution. Electrode potential was converted into reversible hydrogen electrode potential (vs. RHE), and solution IR compensation was performed. The LSV curves of the prepared material were measured at different scanning rates in an inert constant-room-temperature environment to characterize its catalytic hydrogen evolution performance. Electrochemical impedance spectroscopy and scanning CV curves were also measured to obtain the electrochemical surface area.

3. Result and Discussion

Characterization of $Ti_3C_2T_x$

First, the $Ti_3C_2T_x$ was characterized using a Scanning Electron Microscope shown in Figure 2a $Ti_3C_2T_x$ which has prominent layered characteristics, which allows for a large contact area with $MoSe_2$ and CC. However, due to introducing some terminal groups on the surface of Ti_3C_2 during the preparation process, the Raman spectrum was used to

characterize its molecular vibration. As shown in Figure 2b, in addition to its inherent interlayer vibration mode E_g peak, there were three apparent peaks at 235 cm^{-1}, 373 cm^{-1}, and 610 cm^{-1}, which, respectively, represent the vibration modes of terminal groups such as F and OH, which are the same as previously reported [32]. To determine the phase-composition structure of the $Ti_3C_2T_x$, we carried out XRD, as shown in Figure 2c. $Ti_3C_2T_x$ had prominent peaks near 7.3°, 34.9°, 35.2° and 63°, which, respectively, correspond to the (002), (001), (104), (105) crystal planes of Ti_3C_2 [33], and the sharp peak represents its good crystallinity. However, XPS was used further to determine the element composition and valence state of $Ti_3C_2T_x$. As shown in Figure 2d, the XPS full spectra of $Ti_3C_2T_x$ showed distinctive peaks of Ti and OH F, O. The Ti 2p XPS spectra after deconvoluting is shown in Figure 2e, where there are double peaks at lower binding energies of 455.6 eV and higher binding energies of 465 eV were obtained, confirming the existence of oxygen-containing terminal groups, which further confirmed our previous Raman results. The C XPS spectra after deconvoluting are shown in Figure 2f; double peaks at lower binding energies of 284.8 eV and higher binding energies of 281.8 eV were obtained after Gaussian Lorentz fitting. The stoichiometric ratio of Ti and C is about 100:68. However, The $Ti_3C_2T_x$ we obtained was rich in oxygen, hydroxyl, F, and other terminal groups.

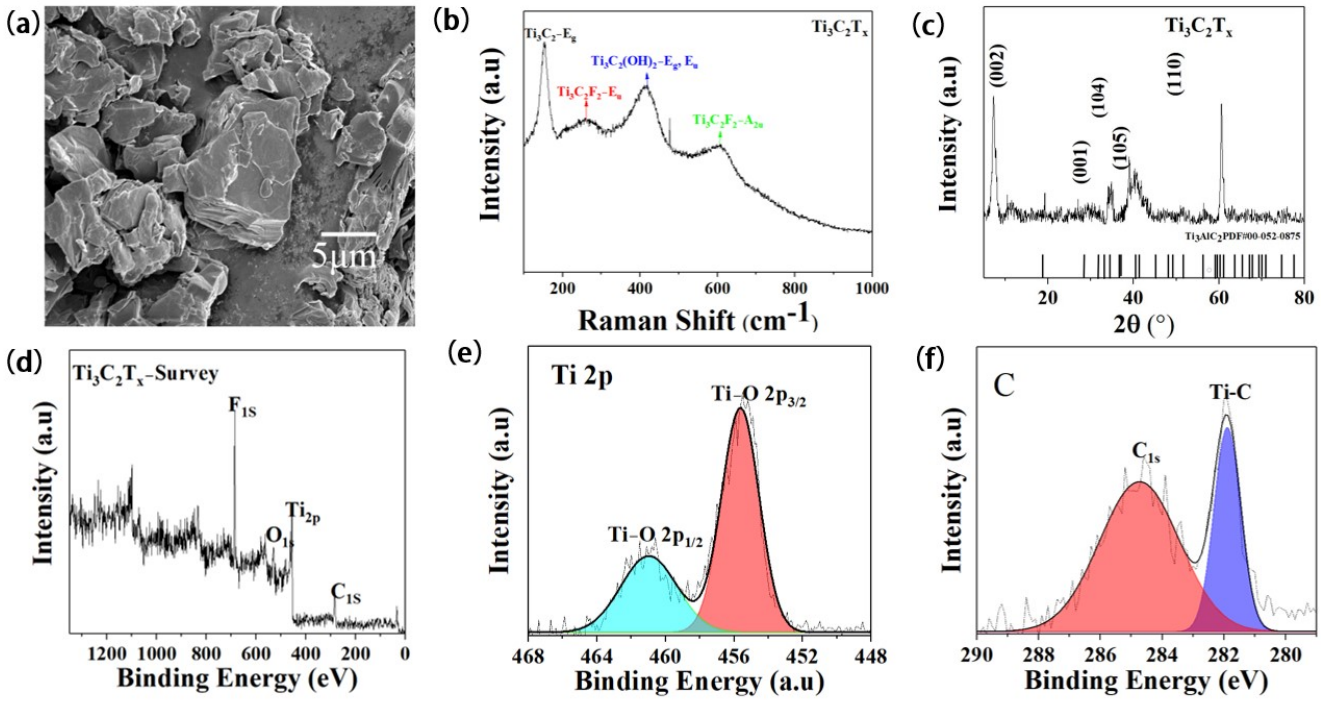

Figure 2. (**a**) SEM image; (**b**) Raman Spectrum; (**c**) XRD; and (**d**–**f**) XPS of $Ti_3C_2T_x$.

$MoSe_2$@$Ti_3C_2T_x$ was successfully synthesized on the Carbon Clothes with a facile one-step hydrothermal. During the preparation of the samples, the $Ti_3C_2T_x$ played a key role, and SEM was used to observe the influence of the $Ti_3C_2T_x$ on the surface morphology features of the synthesized samples. As shown in Figure 3a–c, with the increase of $Ti_3C_2T_x$ content, more and more $MoSe_2$ became attached to the carbon cloth substrate. This may be due to the intense attraction between terminal groups (-F, -OH, -O) on $Ti_3C_2T_x$ and carbon fiber cloth substrate. However, the surface of $MoSe_2$@4 Mg $Ti_3C_2T_x$ had the most evenly distributed $MoSe_2$ nanoflowers. A high-magnification scanning electron microscope was used to analyze its surface morphology further to study the $MoSe_2$@4 Mg $Ti_3C_2T_x$. High-magnification scanning microscope photographs of $MoSe_2$ nanoflowers are shown in Figure 3d–f. The size distribution of a single nanoflower was between 30 and 60 nm.

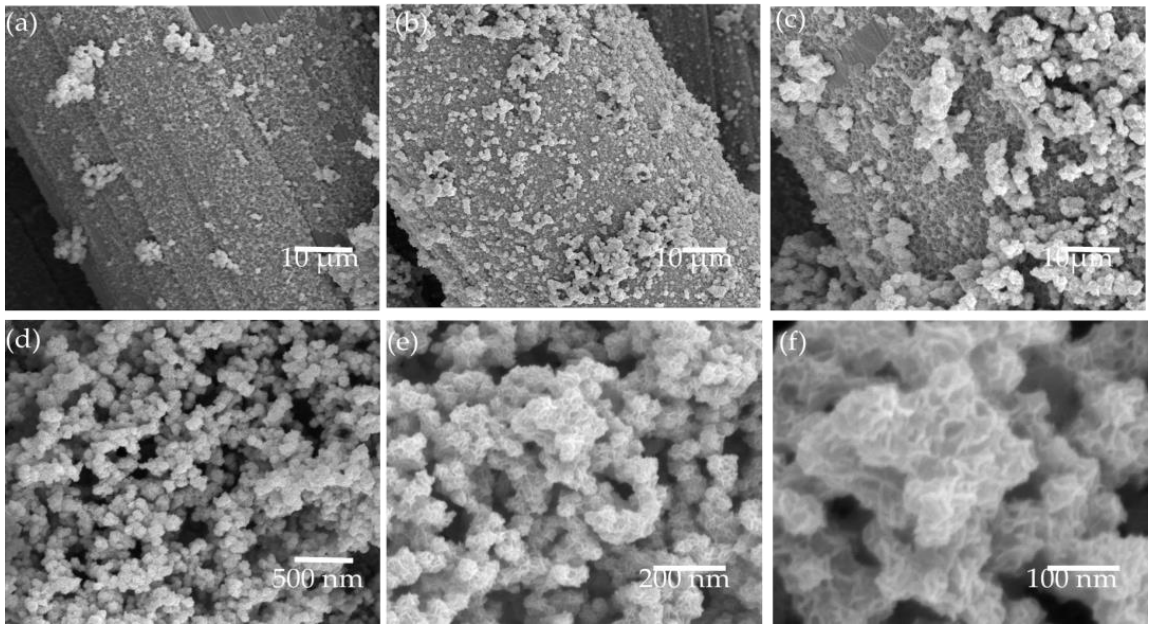

Figure 3. SEM images of synthesized $MoSe_2$@$Ti_3C_2T_x$/CC samples; (**a**) $MoSe_2$@2 mg$Ti_3C_2T_x$/CC; (**b**) $MoSe_2$@4 mg$Ti_3C_2T_x$/CC; (**c**) $MoSe_2$@6 mg$Ti_3C_2T_x$/CC; and $MoSe_2$ nanoflower on the samples of $MoSe_2$@4 mg$Ti_3C_2T_x$/CC at (**d**) ×5000, (**e**) ×100,000, (**f**) ×200,000.

The Raman spectrum of all the samples show a characteristic peak at ≈285.4 cm^{-1}. In accurate compliance to the in-plane ($E^1{}_{2g}$) mode, two other peaks at ≈239.4 cm^{-1} and ≈342.5 cm^{-1} on both sides of the main peak were found, (Figure 4a). Corresponding to A_{1g} and $B^1{}_{2g}$, the characteristic Raman manifested as 2H $MoSe_2$ [34–37]. Furthermore, there are two inconspicuous peaks at ≈194 cm^{-1} and ≈376 cm^{-1}, which correspond to the characteristic Raman mode of 1T $MoSe_2$ [38,39]. However, with the increase of $Ti_3C_2T_x$, there was no apparent shift in each peak position, and no characteristic peak of $Ti_3C_2T_x$ was found in each sample; this may be due to the low amount of $Ti_3C_2T_x$ or the adsorption of $Ti_3C_2T_x$ on the carbon fiber cloth substrate. Raman spectra show that the $MoSe_2$ we synthesized were 1T/2H multiple phases. To ascertain the existing phase composition and structural information of the as-synthesized samples XRD was carried out. The results are shown in Figure 4b; three prominent peaks were found which were located around 13.7°, 31.4° and 58°, respectively. Representing the (002), (110) and (008) crystal planes of $MoSe_2$, due to the presence of surface structural defects, the (002) and (100) peaks of $MoSe_2$ broaden in the XRD pattern [40]. Compared with the 2H-phase $MoSe_2$ (JCPDS No 29–0914), standard XRD pattern means all the sample peaks of the (100) diffraction peaks shift right to a larger angle and the (002) crystal plane shifts left to a smaller angle, which is in good agreement with the result demonstrating the presence of 1T-phase $MoSe_2$ in all synthesized samples [41,42]. With the increase in the amount of $Ti_3C_2T_x$, a prominent peak corresponding to the (110) crystal plane of Ti_3C_2 was observed at 60.5° in $MoSe_2$@4 mg. At $Ti_3C_2T_x$, $MoSe_2$@6 mg $Ti_3C_2T_x$, another peak was observed near 7.3° and in $MoSe_2$@6 mg $Ti_3C_2T_x$, corresponding to the (002) crystal plane of Ti_3C_2. Therefore, we reached the preliminary conclusion that $Ti_3C_2T_x$ did not decompose or participate in the reaction in the $MoSe_2$@$Ti_3C_2T_x$ synthesis. Next, XPS survey spectra illustrate that C, Ti, Mo, and Se elements are uniformly distributed in all samples. Next, the XPS spectra of $MoSe_2$@$Ti_3C_2T_x$ were further investigated for the presence of the 1T phase in the samples. Figure 4c shows the XPS spectrum in the Mo region. Two peaks at 54.7 and 53.7 eV correspond to 1T-phase $MoSe_2$; double peaks at 228.3 and 231.4 eV correspond to Mo within the 1T phase, whereas 55.2 and 54.3 eV are assigned to the 2H phase $MoSe_2$. The other pair at 229.3 eV and 232.5 eV can be assigned to the $3d_{5/2}$ and $3d_{3/2}$ orbitals of Mo within the 2H phase [43,44]. However, the 1T and 2H contents of each sample were different. The 1T-phase content in

$MoSe_2$@2 mg $Ti_3C_2T_x$ was 64.4%; for $MoSe_2$@4 mg $Ti_3C_2T_x$, it was 66.9%; and the 1T-phase content in $MoSe_2$@6 mg $Ti_3C_2T_x$ was 54.58%. However, according to the previous report, temperature plays an important role in the formation of 1T $MoSe_2$ [45]. Theoretically, there should be little difference in the 1T $MoSe_2$ content of the sample. However, the addition of $Ti_3C_2T_x$ may have affected the synthesis of 1T-phase $MoSe_2$, but the terminal groups of $Ti_3C_2T_x$ may prevent the formation of $MoSe_2$. All the XPS results verified that 1T and 2H phases coexist in the samples we synthesized.

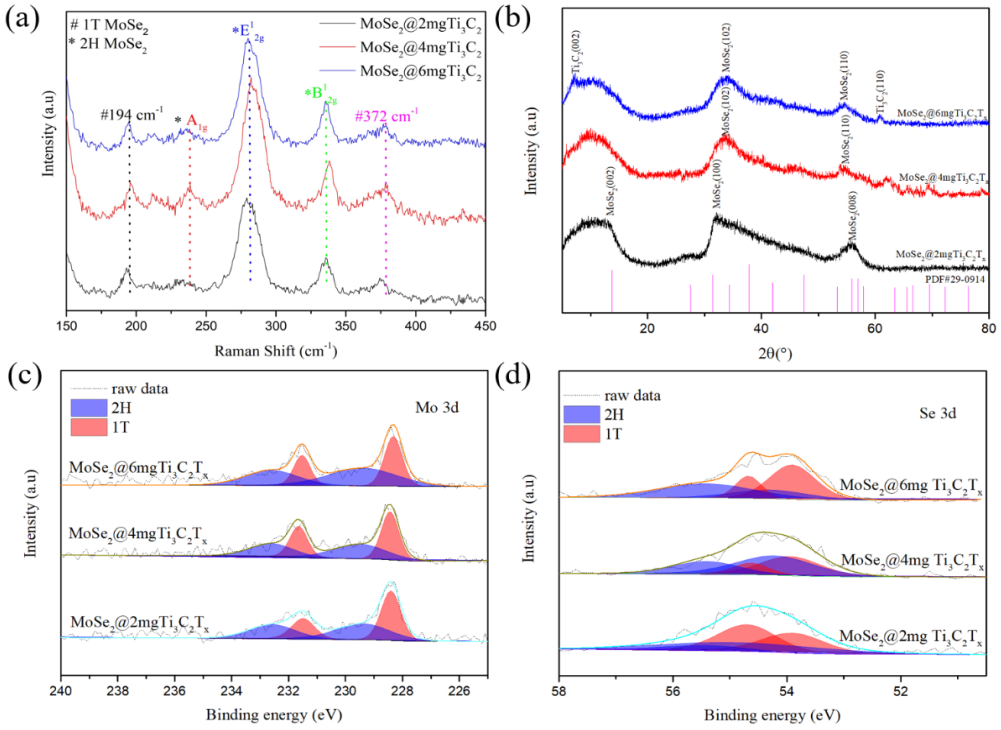

Figure 4. $MoSe_2$ synthesized with different $Ti_3C_2T_x$-added amounts; (**a**) Raman spectrometer shifts; (**b**) XRD pattern; (**c**) Mo 3d XPS spectra; and (**d**) Se 3d XPS spectra.

We first tested the LSV curves for bare CC and MXene on CC, as shown in Figure 5. Dropping a small amount of MXene onto the carbon cloth can significantly improve the catalytic performance of the carbon cloth by about 2 mg. This may be due to the good conductivity of MXene. In addition, to determine the stability of MXene on the carbon cloth, we used a similar method in the paper 1000 CV cycles, and the performance of the sample did not change significantly. This may be due to the strong adsorption ability of MXene as a nanosheet and CC substrate, which did not considerably detach during the catalytic process. The HER electrochemical catalytic properties of $MoSe_2$ obtained with a diverse mass of $Ti_3C_2T_x$ were investigated in Figure 6a. According to XPS, the polarization curves after IR calibration are our work's best value when the mass of $Ti_3C_2T_x$ was 4 mg. The overpotential of η@10 mA/cm^2 was 184. 4 mV. Still, with the increase of the $Ti_3C_2T_x$, the overpotential of @6 mg $Ti_3C_2T_x$ drops to 244.8 mV. This is due to its low 1T-phase content. However, compared with the sample without $Ti_3C_2T_x$, using different masses of $Ti_3C_2T_x$ suggests that the existence of $Ti_3C_2T_x$ plays an important role in the majorization of HER electrocatalytic performance. The Tafel slope reflecting chemical reactivity in the HER further confirms the above results. Derived from their corresponding polarization curves, the samples prepared under different conditions are displayed in Figure 6b. The Tafel slope significantly decreased (79 mV dec^{-1}), indicating a faster HER process in the sample. To understand the difference in the HER catalytic performance of the samples we synthesized varied $Ti_3C_2T_x$ amounts in the Heyrovsky reaction rate-resolving stage. Furthermore, we analyzed CV measurement results to evaluate the effective electrochemical activity surface area (ECSA) by measuring C_{dl} stemming.

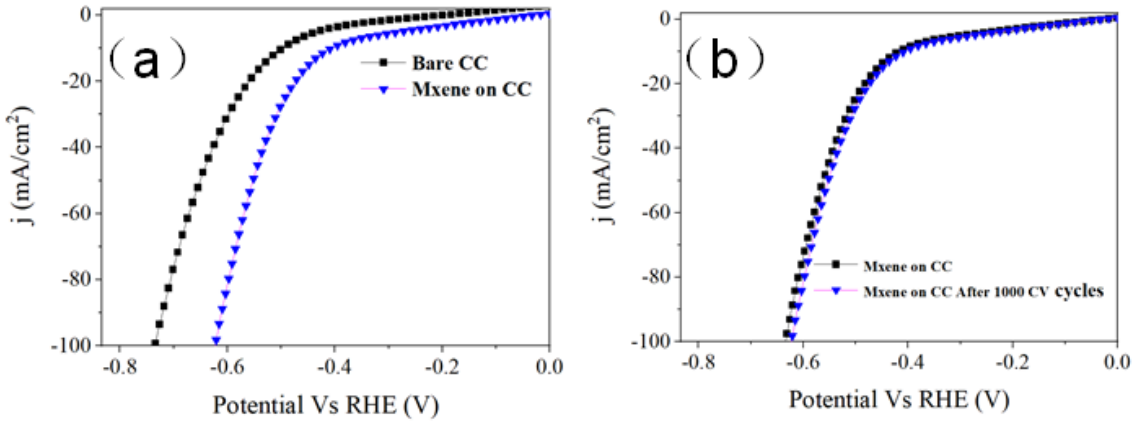

Figure 5. (**a**) LSV of Bare CC and MXene on CC; (**b**) LSV of MXene on CC and MXene on CC after 1000 CV cycles.

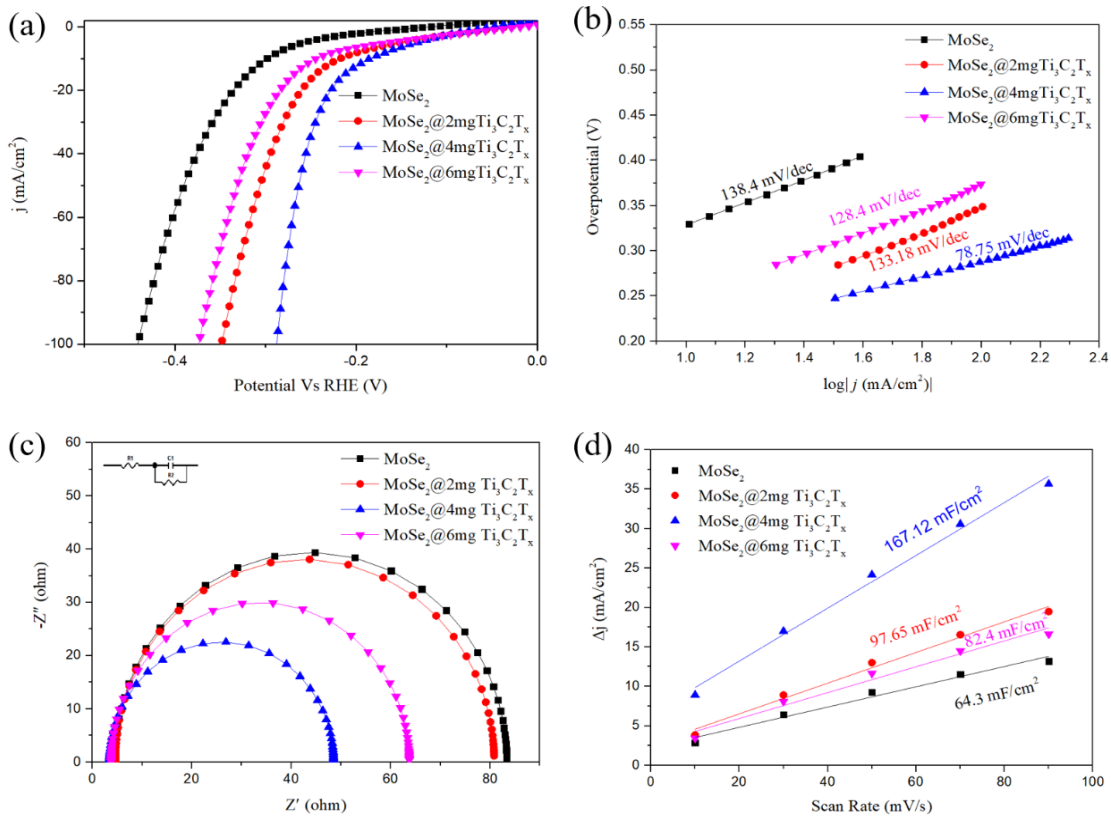

Figure 6. Electrochemical properties of $MoSe_2$@ $Ti_3C_2T_x$ synthesized with diverse amount of $Ti_3C_2T_x$. (**a**) Polarization curves after IR calibration; (**b**) corresponding Tafel plots of the samples stemming from (**a**); (**c**) Nyquist plots of the samples; and (**d**) C_{dl} current at different scan rates.

Samples with different component structures' capacitive current and scan rates are presented in Figure 6c. $MoSe_2$@4 mg-$Ti_3C_2T_x$ also manifested larger C_{dl} (167.12 mF cm^{-2}). Because of the existence of surface structural defects, the composite phase structure exposes more active site, which improves the performance of electrocatalytic HER. EIS tests were also conducted further to understand the electrochemical behavior in the HER process. Figure 6d presents the Nyquist plots of tested samples, displaying stable-system semicircle features. The charge-transfer resistance (R_{ct}) can be obtained by calculating and fitting the Nyquist plot of Figure 6c. The R_{ct} values $MoSe_2$@4 mg-$Ti_3C_2T_x$ (23 Ω), $MoSe_2$@2 mg-$Ti_3C_2T_x$ (39 Ω), $MoSe_2$@6 mg-$Ti_3C_2T_x$ (30 Ω), and $MoSe_2$ (40 Ω) results as

mentioned above expound that the addition of $Ti_3C_2T_x$ is critical to enhancing HER catalytic activity. From work obtained samples, $MoSe_2$@4 mg$Ti_3C_2T_x$ that exhibit the best HER electrocatalytic performance.

The double plate capacitance extracted in the nonfaradaic-zone CV cycle is proportional to the electrochemical activation area of the catalytic electrode. Figure 7 shows the cyclic voltammetry curve of the sample for different $MoSe_2$@$Ti_3C_2T_x$. The sample was subjected to cyclic voltammetry testing. The test solution was consistent with the previous electrochemical workstation and still used a 0.5 mol/L H_2SO_4 solution. The scanning rates were 10, 30, 50, 70, and 90 mV/s. In addition, to ensure the stability of the sample, the last one was selected for 100 cycles at each rate and plotted. As shown in Figure 7a, the $MoSe_2$ sample electrode without adding $Ti_3C_2T_x$ showed the smallest capacitive behavior, followed by the electrode sample with the added 2 mg $Ti_3C_2T_x$. As the content of $Ti_3C_2T_x$ increases, the area of the CV curve gradually increases. The sample with a dosage of 4 mg $Ti_3C_2T_x$ has the largest CV area. When the dosage of $Ti_3C_2T_x$ is further increased to 6 mg, the geometric area of the CV curve shows a significant reduction trend. This indicates that the doping amount of $Ti_3C_2T_x$ has an optimal value. When the doping amount of $Ti_3C_2T_x$ reaches an optimal value, its catalytic activity will exceed the contribution of the carbon cloth matrix, becoming the dominant role instead. However, its performance will gradually decline after exceeding a specific optimization interval. Based on the previous XPS characterization results, this is due to the addition of a large amount of $Ti_3C_2T_x$, which is affected by the adsorption of terminal groups -F, -OH, etc., on the surface of $Ti_3C_2T_x$. The solution's environment during the preparation of 1T phase is disrupted, thereby affecting the generation of 1T-phase $MoSe_2$, and reducing the content of 1T phase in the sample. In addition, due to the reduction of $MoSe_2$ content in the 1T phase, the number of hydrogen evolution catalytic active sites introduced by the disordered arrangement of atoms at the interface of 1T and 2H phase in the sample due to different structures, will also be reduced. This further affects its catalytic activity and reduces the CV area at different scanning rates.

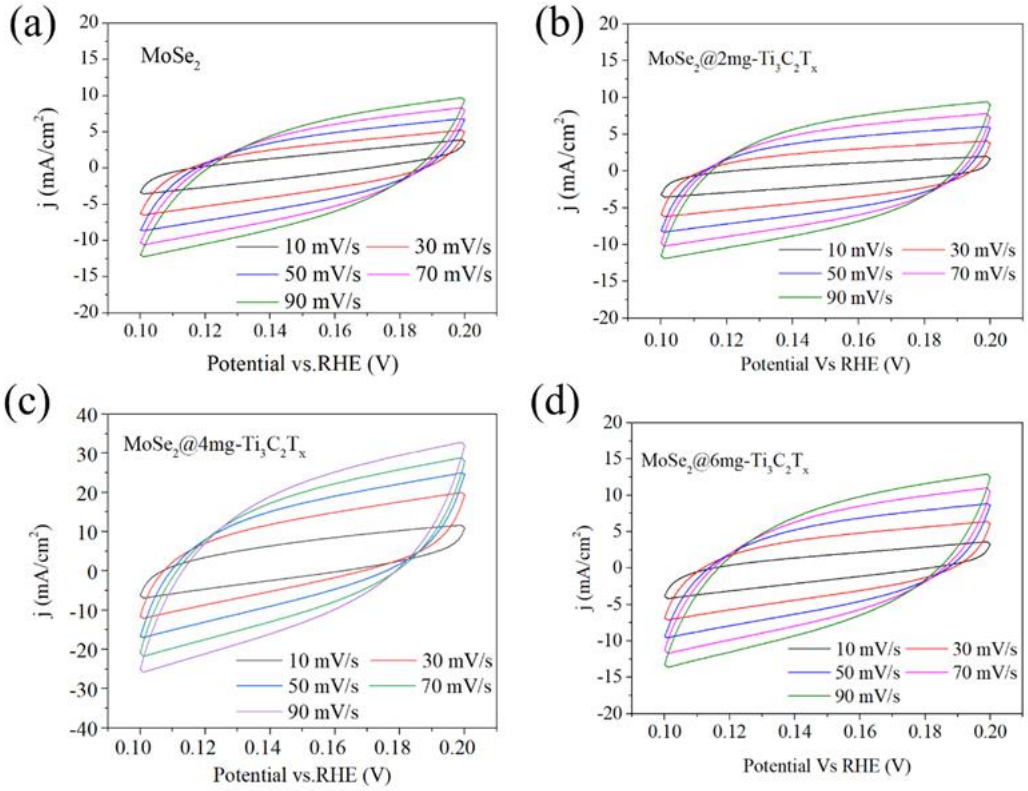

Figure 7. CV scanning curve in the scanning range of 0.1 V–0.2 V for different samples of (**a**) $MoSe_2$, (**b**) $MoSe_2$@2 mg-$Ti_3C_2T_x$, (**c**) $MoSe_2$@4 mg-$Ti_3C_2T_x$, and (**d**) $MoSe_2$@6 mg-$Ti_3C_2T_x$.

We investigated the catalytic performance of $Ti_3C_2T_x$ during the in situ growth of $MoSe_2$ electrodes on carbon cloth. The results showed that adding $Ti_3C_2T_x$ optimized the electrocatalytic hydrogen evolution performance of $MoSe_2$ electrodes to varying degrees. Based on characterization methods, it is speculated that adding $Ti_3C_2T_x$ changed the in situ growth process of $MoSe_2$ on carbon cloth. Due to the introduction of active groups, such as F during the preparation of $Ti_3C_2T_x$, it is more inclined to adhere to the carbon cloth. On the other hand, as a two-dimensional material, it is easy to synthesize heterostructures with $MoSe_2$ based on the interlayer van der Waals force. In addition, its natural good conductivity can act as a good electronic channel between $MoSe_2$ and the carbon cloth. Therefore, $MoSe_2$ not only exposes more electrocatalytic active sites but also greatly improves the adhesion between the catalyst and the carbon cloth, so it can effectively optimize the electrocatalytic performance of $MoSe_2$. Based on the successful preparation of 1T/2H impure-phase $MoSe_2$, we investigated the effect of $Ti_3C_2T_x$ addition on the electrocatalytic performance of $MoSe_2$. For samples with a low amount of $Ti_3C_2T_x$ addition, $Ti_3C_2T_x$ cannot perform its expected conductivity, and the optimization of $MoSe_2$ electrocatalytic performance is limited. However, when more $Ti_3C_2T_x$ is added, the terminal groups adsorbed on the surface of $Ti_3C_2T_x$ will affect the formation of 1T-phase $MoSe_2$. With the increase of $Ti_3C_2T_x$ addition, the sample with 4 mg $Ti_3C_2T_x$ exhibited good electrocatalytic hydrogen evolution performance.

As shown in Table 1, the enhanced catalytic performance is attributed to a larger density of exposed catalytically active edge sites and a higher electrical conductivity. Other studies on improved catalytic activity of $MoSe_2$ have shown that the structure of the high-content 1T phase with defects is instrumental in enhancing HER performance [46].

Table 1. Electrochemical performance (j = 10 mA cm^{-2}) comparison of different $MoSe_2$-based composite samples.

Sample	Overpotential (V vs. RHE)	Tafel Slope ($mV\ dec^{-1}$)	References
2H $MoSe_2$	0.300	82	[47]
$MoSe_2$-amorphous CNT	0.254	49	[48]
C@$MoSe_2$	0.270	72	[49]
Graphene-carbon nanotube aerogel-$MoSe_2$ hybrid	0.228	68	[50]
N-doped RGO/$MoSe_2$ composites	0.229	78	[51]
$MoSe_2/Ti_3C_2T_x$	0.185	79	This work

To study the stability of the sample, we conducted experiments on the stability of the samples $MoSe_2$@$Ti_3C_2T_x$. After the CV test, the following experiments were carried out: the SEM of samples shown in Figure 8a, and the sample Raman spectroscopy shown in Figure 8b. There were no shifts for the Raman peak of 1T and 2H $MoSe_2$ after the test, and the main crystal planes remain the same as before the CV test as shown in Figure 8c, and the half-peak width did not change significantly, indicating that the test did not significantly change its crystal structure. We used XPS to illustrate whether $MoSe_2$ transitioned from 1T to 2H after the test, since phase 2H is a thermodynamically stable phase. As shown in the figure, the chemical elements and valence states that the full spectrum of XPS did not change significantly, and in spectroscopy, we used the same method as in the paper to split the Mo 3d and Se 3d peaks, respectively. However, the phase content in $MoSe_2$@2 mg $Ti_3C_2T_x$ after the CV test decreased from 64.4% to 63.3%. This reduction is tolerable since the samples were dried before testing.

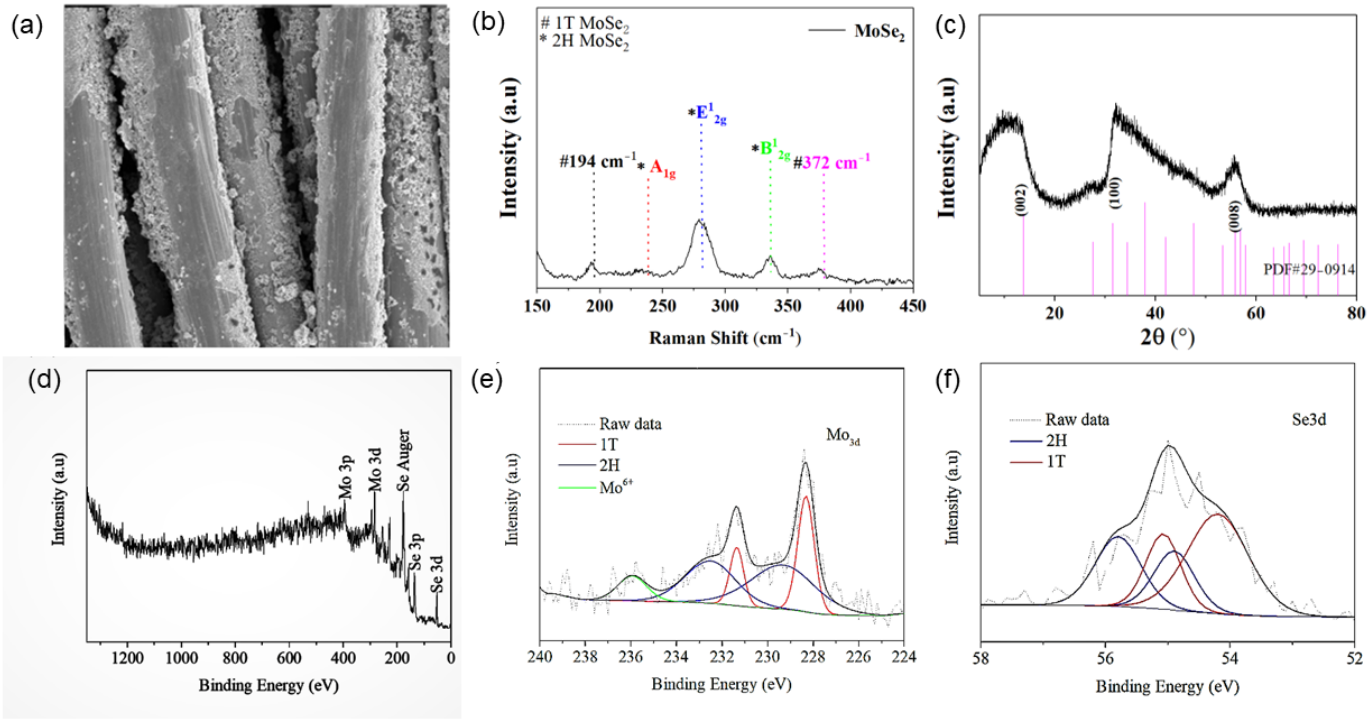

Figure 8. Characterization of MoSe2@2 mg $Ti_3C_2T_x$ after CV test samples of (**a**) SEM, (**b**) Raman spectrum, (**c**) XRD spectrum, (**d**) XPS full spectrum, (**e**) XPS Mo 3d peak, and (**f**) XPS Se 3d peak.

In addition, the surface morphology of the samples after different cycles was observed. Figure 9a–c show the initial morphology of the sample without cycling. It can be seen that a large number of $MoSe_2$ clusters uniformly adhere to the surface of the sample, and there is also a small amount of $MoSe_2$ powder attached to the surface of the carbon cloth fiber. Still the contribution to hydrogen evolution performance is extremely limited due to the small contact area with the carbon cloth. A clear tissue network can be seen with significant adhesion to the substrate at high magnification. Figure 9d–f shows the surface morphology of the sample after 500 cycles, and $MoSe_2$ powder on the surface of the carbon cloth has obviously fallen off. Still, the $MoSe_2$ clusters adsorbed on the surface have not obviously fallen off. Still the cluster morphology has changed greatly, the $MoSe_2$ on the surface has changed from loose nanoflower clusters to "chocolate" like whole blocks attached to the surface of the carbon cloth, and small $MoSe_2$ particles can still be seen at local magnification. The particles are closely bound to the carbon cloth substrate. In Figure 9g–i, a large number of $MoSe_2$ nanoparticles are still uniformly adhered to the surface of the sample after 1000 cycles. However, the difference is that the particle size is significantly reduced under local magnification, with a small amount of detachment locally. Overall, the majority of $MoSe_2$ has a relatively tight binding force. It is worth noting that Nafion and other reagents were not used to promote the adhesion of $MoSe_2$ on the substrate during this experimental testing process. The small amount of $MoSe_2$ attached to the surface of the carbon cloth itself has a limited contribution to the catalytic performance of the catalyst due to its small interface with the carbon cloth, and its detachment will not significantly impact the catalyst performance.

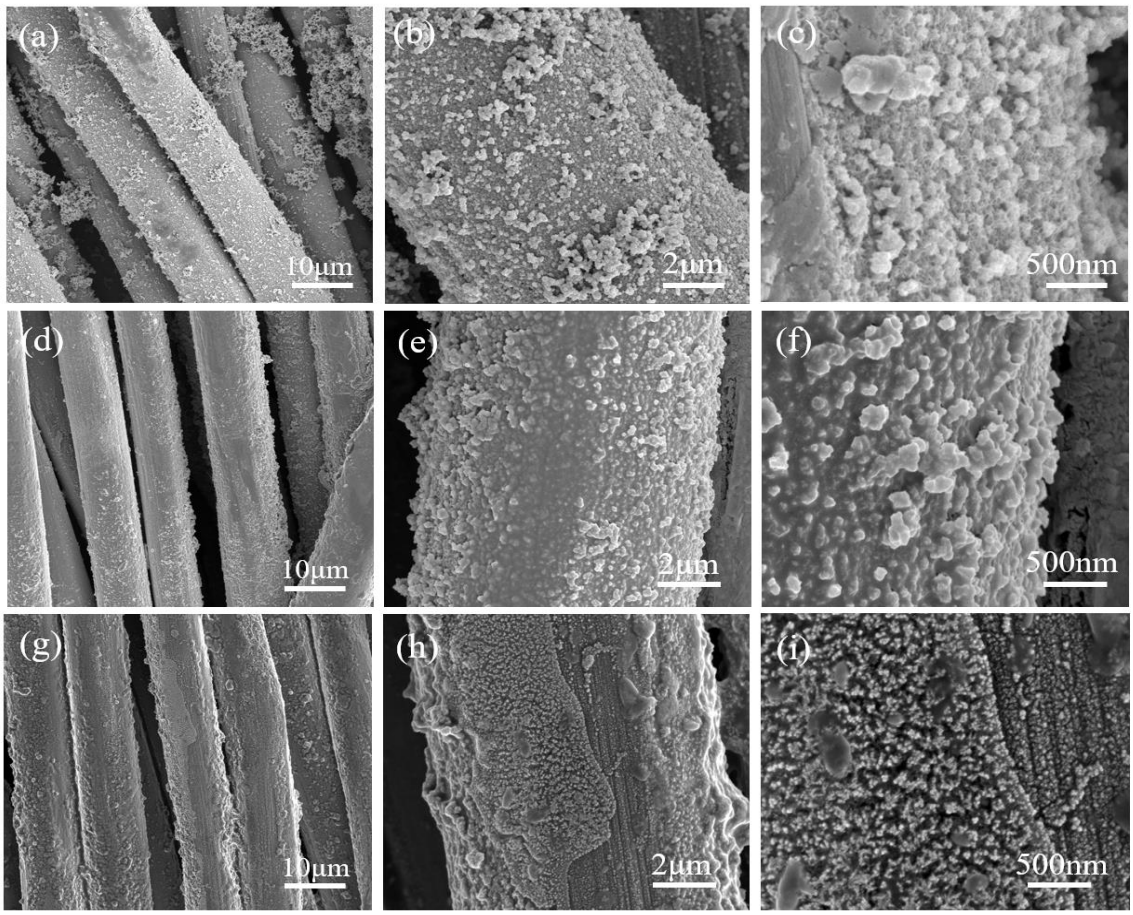

Figure 9. (**a**–**c**) Carbon cloth in situ growth $MoSe_2$@4 mg $Ti_3C_2T_x$ initial surface morphology of sample (**d**–**f**) after 500 Cycles, and microscopic morphology of the sample at different magnification times, and (**g**–**i**) after 1000 cycles, and microscopic morphology of the sample at different magnification times.

4. Conclusions

In this work, the two-dimensional $Ti_3C_2T_x$ was added to form the heterostructure with 1T/2H $MoSe_2$ to improve the contact with the conductive carbon fiber cloth substrate. In addition, $Ti_3C_2T_x$ itself, as a good conductor, can provide fast channels and more active sites for electron transfer during electrochemical reactions. According to the control, the addition of a mass of $Ti_3C_2T_x$ to form proper $MoSe_2/Ti_3C_2T_x$ heterostructures with low overpotentials (−185.29 mV) and small Tafel slopes (79 mV dec^{-1}) are achieved with the obtained $MoSe_2$@4 mg-$Ti_3C_2T_x$, Moreover, phase engineering synergistic effects and remaking heterostructures using $MoSe_2$ with other materials can also be used for $MoSe_2$ future development in the field of electrochemical catalysis. However, how the terminal groups of $Ti_3C_2T_x$ influence the formation of the 1T $MoSe_2$ is still not clear. More comparative experiments need to be carried out with further $Ti_3C_2T_x$ addition.

Author Contributions: Conceptualization, Y.W. and J.W.; Methodology, Y.W. and J.W.; Software, Q.Y.; Formal analysis, L.X.; investigation, Q.Y.; Data curation, X.Z.; Writing—original draft, L.X.; writing-review and editing, Y.W. and J.W. All authors have read and agreed to the published version of the manuscript.

Funding: This research received no external funding.

Informed Consent Statement: Not applicable.

Data Availability Statement: Not applicable.

Conflicts of Interest: The authors declare no conflict of interest.

References

1. Seh, Z.W.; Kibsgaard, J.; Dickens, C.F.; Chorkendorff, I.B.; Nørskov, J.K.; Jaramillo, T.F. Combining theory and experiment in electrocatalysis: Insights into materials design. *Science* **2017**, *355*, eaad4998. [CrossRef] [PubMed]
2. Schlapbach, L.; Züttel, A. Hydrogen-storage materials for mobile applications. *Nature* **2001**, *414*, 353–358. [CrossRef] [PubMed]
3. Wang, X.; Maeda, K.; Thomas, A.; Takanabe, K.; Xin, G.; Carlsson, J.M.; Domen, K.; Antonietti, M. A metal-free polymeric photocatalyst for hydrogen production from water under visible light. *Nat. Mater.* **2009**, *8*, 76–80. [CrossRef] [PubMed]
4. Bodhankar, P.M.; Sarawade, P.B.; Kumar, P.; Vinu, A.; Kulkarni, A.P.; Lokhande, C.D.; Dhawale, D.S. Nanostructured Metal Phosphide Based Catalysts for Electrochemical Water Splitting: A Review. *Small* **2022**, *18*, 2107572. [CrossRef]
5. Luo, Y.; Zhang, Z.; Chhowalla, M.; Liu, B. Recent Advances in Design of Electrocatalysts for High-Current-Density Water Splitting. *Adv. Mater.* **2021**, *34*, 2108133. [CrossRef]
6. Cabán-Acevedo, M.; Stone, M.L.; Schmidt, J.R.; Thomas, J.G.; Ding, Q.; Chang, H.C.; Tsai, M.L.; He, J.H.; Jin, S. Efficient hydrogen evolution catalysis using ternary pyrite-type cobalt phosphosulphide. *Nat. Mater.* **2015**, *14*, 1245–1251. [CrossRef]
7. Mahmood, J.; Li, F.; Jung, S.M.; Okyay, M.S.; Ahmad, I.; Kim, S.J.; Park, N.; Jeong, H.Y.; Baek, J.B. An efficient and pH-universal ruthenium-based catalyst for the hydrogen evolution reaction. *Nat. Nanotechnol.* **2017**, *12*, 441–446. [CrossRef]
8. Han, X.; Wu, X.; Deng, Y.; Liu, J.; Lu, J.; Zhong, C.; Hu, W. Ultrafine Pt Nanoparticle-Decorated Pyrite-Type CoS_2 Nanosheet Arrays Coated on Carbon Cloth as a Bifunctional Electrode for Overall Water Splitting. *Adv. Energy Mater.* **2018**, *8*, 1800935. [CrossRef]
9. Zhao, Z.; Liu, H.; Gao, W.; Xue, W.; Liu, Z.; Huang, J.; Pan, X.; Huang, Y. Surface-Engineered PtNi-O Nanostructure with Record-High Performance for Electrocatalytic Hydrogen Evolution Reaction. *J. Am. Chem. Soc.* **2018**, *140*, 9046–9050. [CrossRef]
10. Jaramillo, T.F.; Jørgensen, K.P.; Bonde, J.; Nielsen, J.H.; Horch, S.; Chorkendorff, I. Identification of Active Edge Sites for Electrochemical H_2 Evolution from MoS_2 Nanocatalysts. *Science* **2007**, *317*, 100–102. [CrossRef]
11. Fu, Q.; Han, J.; Wang, X.; Xu, P.; Yao, T.; Zhong, J.; Zhong, W.; Liu, S.; Gao, T.; Zhang, Z.; et al. 2D Transition Metal Dichalcogenides: Design, Modulation, and Challenges in Electrocatalysis. *Adv. Mater.* **2021**, *33*, 1907818. [CrossRef] [PubMed]
12. Voiry, D.; Yang, J.; Chhowalla, M. Recent Strategies for Improving the Catalytic Activity of 2D TMD Nanosheets Toward the Hydrogen Evolution Reaction. *Adv. Mater.* **2016**, *28*, 6197–6206. [CrossRef] [PubMed]
13. Zhang, Z.; Wang, J.; Li, Y.; Zhang, S.; Xiao, L.; Wang, J.; Qi, J. Hydrothermal preparation of MoX_2 (X = S, Se, Te)/TaS_2 hybrid materials on carbon cloth as efficient electrocatalyst for hydrogen evolution reaction. *Int. J. Hydrogen Energy* **2023**, *48*, 4207–4219. [CrossRef]
14. Deng, S.; Zhong, Y.; Zeng, Y.; Wang, Y.; Yao, Z.; Yang, F.; Lin, S.; Wang, X.; Lu, X.; Xia, X.; et al. Directional Construction of Vertical Nitrogen-Doped 1T-2H $MoSe_2$/Graphene Shell/Core Nanoflake Arrays for Efficient Hydrogen Evolution Reaction. *Adv. Mater.* **2017**, *29*, 1700748. [CrossRef]
15. Xu, C.; Peng, S.; Tan, C.; Ang, H.; Tan, H.; Zhang, H.; Yan, Q. Ultrathin S-doped $MoSe_2$ nanosheets for efficient hydrogen evolution. *J. Mater. Chem. A* **2014**, *2*, 5597–5601. [CrossRef]
16. Najafi, L.; Bellani, S.; Oropesa-Nuñez, R.; Ansaldo, A.; Prato, M.; Del Rio Castillo, A.E.; Bonaccorso, F. Doped-$MoSe_2$ Nanoflakes/3d Metal Oxide–Hydr(Oxy)Oxides Hybrid Catalysts for pH-Universal Electrochemical Hydrogen Evolution Reaction. *Adv. Energy Mater.* **2018**, *8*, 1801764. [CrossRef]
17. Chen, X.; Qiu, Y.; Liu, G.; Zheng, W.; Feng, W.; Gao, F.; Cao, W.; Fu, Y.; Hu, W.; Hu, P. Tuning electrochemical catalytic activity of defective 2D terrace $MoSe_2$ heterogeneous catalyst via cobalt doping. *J. Mater. Chem. A* **2017**, *5*, 11357–11363. [CrossRef]
18. Qian, J.; Wang, T.; Xia, B.; Xi, P.; Gao, D. Zn-doped $MoSe_2$ nanosheets as high-performance electrocatalysts for hydrogen evolution reaction in acid media. *Electrochim. Acta* **2019**, *296*, 701–708. [CrossRef]
19. Ambrosi, A.; Sofer, Z.; Pumera, M. 2H $\rightarrow$ 1T phase transition and hydrogen evolution activity of MoS_2, $MoSe_2$, WS_2 and WSe_2 strongly depends on the MX_2 composition. *Chem. Commun.* **2015**, *51*, 8450–8453. [CrossRef]
20. Deng, S.; Yang, F.; Zhang, Q.; Zhong, Y.; Zeng, Y.; Lin, S.; Wang, X.; Lu, X.; Wang, C.Z.; Gu, L.; et al. Phase Modulation of (1T-2H)-$MoSe_2$/TiC-C Shell/Core Arrays via Nitrogen Doping for Highly Efficient Hydrogen Evolution Reaction. *Adv. Mater.* **2018**, *30*, 1802223. [CrossRef]
21. Jiang, M.; Zhang, J.; Wu, M.; Jian, W.; Xue, H.; Ng, T.W.; Lee, C.S.; Xu, J. Synthesis of 1T-$MoSe_2$ ultrathin nanosheets with an expanded interlayer spacing of 1.17 nm for efficient hydrogen evolution reaction. *J. Mater. Chem. A* **2016**, *4*, 14949–14953. [CrossRef]
22. Wang, L.; Zeng, Z.; Gao, W.; Maxson, T.; Raciti, D.; Giroux, M.; Pan, X.; Wang, C.; Greeley, J. Tunable intrinsic strain in two-dimensional transition metal electrocatalysts. *Science* **2019**, *363*, 870–874. [CrossRef] [PubMed]
23. Wang, P.; Wang, B. Designing Self-Supported Electrocatalysts for Electrochemical Water Splitting: Surface/Interface Engineering toward Enhanced Electrocatalytic Performance. *ACS Appl. Mater. Interfaces* **2021**, *13*, 59593–59617. [CrossRef] [PubMed]
24. Lin, Z.; Lin, B.; Wang, Z.; Chen, S.; Wang, C.; Dong, M.; Gao, Q.; Shao, Q.; Ding, T.; Liu, H.; et al. Facile Preparation of 1T/2H-Mo($S_{1-x}Se_x$)$_2$ Nanoparticles for Boosting Hydrogen Evolution Reaction. *ChemCatChem* **2019**, *11*, 2217–2222. [CrossRef]
25. Gong, Q.; Cheng, L.; Liu, C.; Zhang, M.; Feng, Q.; Ye, H.; Zeng, M.; Xie, L.; Liu, Z.; Li, Y. Ultrathin $MoS_{2(1-x)}Se_{2x}$ Alloy Nanoflakes For Electrocatalytic Hydrogen Evolution Reaction. *ACS Catal.* **2015**, *5*, 2213–2219. [CrossRef]
26. Kwak, I.H.; Kwon, I.S.; Lee, J.H.; Lim, Y.R.; Park, J. Chalcogen-vacancy group VI transition metal dichalcogenide nanosheets for electrochemical and photoelectrochemical hydrogen evolution. *J. Mater. Chem. C* **2021**, *9*, 101–109. [CrossRef]

27. Zhou, X.; Liu, Y.; Ju, H.; Pan, B.; Zhu, J.; Ding, T.; Wang, C.; Yang, Q. Design and Epitaxial Growth of $MoSe_2$–NiSe Vertical Heteronanostructures with Electronic Modulation for Enhanced Hydrogen Evolution Reaction. *Chem. Mater.* **2016**, *28*, 1838–1846. [CrossRef]
28. Tang, X.; Zhang, J.Y.; Mei, B.; Zhang, X.; Liu, Y.; Wang, J.; Li, W. Synthesis of hollow $CoSe_2$/$MoSe_2$ nanospheres for efficient hydrazine-assisted hydrogen evolution. *Chem. Eng. J.* **2021**, *404*, 126529. [CrossRef]
29. Inta, H.R.; Ghosh, S.; Mondal, A.; Tudu, G.; Koppisetti, H.V.; Mahalingam, V. $Ni_{0.85}Se$/$MoSe_2$ Interfacial Structure: An Efficient Electrocatalyst for Alkaline Hydrogen Evolution Reaction. *ACS Appl. Energy Mater.* **2021**, *4*, 2828–2837. [CrossRef]
30. Zhang, Y.; Zhang, S.; He, Y.; Li, H.; He, T.; Shi, H.; Ma, X.; Yang, Q.; Chen, L.; Chen, J. Self-supporting $MoSe_2$/$CoSe_2$@CFP electrocatalyst electrode for high-efficiency HER under alkaline solution. *J. Solid State Chem.* **2021**, *298*, 122108. [CrossRef]
31. Mahmood, A.; Khan, S.; Rahayu, F.; Shah, A.U.H.A.; Rahman, A.U.; Muhammad, T.; Khan, A.; Ullah, N. Factors Effecting and Structural Engineering of Molybdenum Nitride-Based Electrocatalyst for Overall Water Splitting: A Critical Review. *Energy Technol.* **2023**, *11*, 2194–4288. [CrossRef]
32. Zhang, S.; Ying, H.; Huang, P.; Yang, T.; Han, W.Q. Hierarchical utilization of raw $Ti_3C_2T_x$ MXene for fast preparation of various $Ti_3C_2T_x$ MXene derivatives. *Nano Res.* **2022**, *15*, 2746–2755. [CrossRef]
33. Chen, B.; Feng, A.; Liu, K.; Wu, J.; Yu, Y.; Song, L. High-performance capacitive deionization using 3D porous $Ti_3C_2T_x$ with improved conductivity. *J. Electroanal. Chem.* **2021**, *895*, 115515. [CrossRef]
34. Qi, Z.; Wang, S.; Li, Y.; Wang, L.; Zhao, L.; Ge, Q.; Zhang, J.Z. Scavenging activity and reaction mechanism of $Ti_3C_2T_x$ MXene as a novel free radical scavenger. *Ceram. Int.* **2021**, *47*, 16555–16561. [CrossRef]
35. Alhabeb, M.; Maleski, K.; Anasori, B.; Lelyukh, P.; Clark, L.; Sin, S.; Gogotsi, Y. Guidelines for Synthesis and Processing of Two-Dimensional Titanium Carbide ($Ti_3C_2T_x$ MXene). *Chem. Mater.* **2017**, *29*, 7633–7644. [CrossRef]
36. Li, C.; Zhu, L.; Li, H.; Li, H.; Wu, Z.; Liang, C.; Zhu, X.; Sun, Y. Dual surfactants applied in synthesis of $MoSe_2$ for high-efficiency hydrogen evolution reaction. *J. Alloys Compd.* **2021**, *863*, 158092. [CrossRef]
37. Truong, Q.D.; Nakayasu, Y.; Nguyen, Q.T.; Nguyen, D.N.; Nguyen, C.T.; Devaraju, M.K.; Rangappa, D.; Nayuki, K.; Sasaki, Y.; Tran, P.D.; et al. Defect-rich exfoliated $MoSe_2$ nanosheets by supercritical fluid process as an attractive catalyst for hydrogen evolution in water. *Appl. Surf. Sci.* **2020**, *505*, 144537. [CrossRef]
38. Zhao, X.; Zhao, Y.; Huang, B.; Cai, W.; Sui, J.; Yang, Z.; Wang, H.E. $MoSe_2$ nanoplatelets with enriched active edge sites for superior sodium-ion storage and enhanced alkaline hydrogen evolution activity. *Chem. Eng. J.* **2020**, *382*, 123047. [CrossRef]
39. Ullah, N.; Xie, M.; Hussain, S.; Yaseen, W.; Shah, S.A.; Yusuf, B.A.; Oluigbo, C.J.; Rasheed, H.U.; Xu, Y.; Xie, J. Simultaneous synthesis of bimetallic@3D graphene electrocatalyst for HER and OER. *Front. Mater. Sci.* **2021**, *15*, 305–315. [CrossRef]
40. Setayeshgar, S.; Karimipour, M.; Molaei, M.; Moghadam, M.R.; Khazraei, S. Synthesis of scalable 1T/2H–$MoSe_2$ nanosheets with a new source of Se in basic media and study of their HER activity. *Int. J. Hydrogen Energy* **2020**, *45*, 6090–6101. [CrossRef]
41. Yin, Y.; Zhang, Y.; Gao, T.; Yao, T.; Zhang, X.; Han, J.; Wang, X.; Zhang, Z.; Xu, P.; Zhang, P.; et al. Synergistic Phase and Disorder Engineering in 1T-$MoSe_2$ Nanosheets for Enhanced Hydrogen-Evolution Reaction. *Adv. Mater.* **2017**, *29*, 1700311. [CrossRef] [PubMed]
42. Shi, H.; Zhang, H.; Li, M.; Wang, Y.; Wang, D. Nanoflower-like 1T/2H mixed-phase $MoSe_2$ as an efficient electrocatalyst for hydrogen evolution. *J. Alloys Compd.* **2021**, *878*, 160381. [CrossRef]
43. Zhang, J.; Chen, Y.; Liu, M.; Du, K.; Zhou, Y.; Li, Y.; Wang, Z.; Zhang, J. 1T@2H-$MoSe_2$ nanosheets directly arrayed on Ti plate: An efficient electrocatalytic electrode for hydrogen evolution reaction. *Nano Res.* **2018**, *11*, 4587–4598. [CrossRef]
44. Li, N.; Wu, J.; Lu, Y.; Zhao, Z.; Zhang, H.; Li, X.; Zheng, Y.Z.; Tao, X. Stable multiphasic 1T/2H $MoSe_2$ nanosheets integrated with 1D sulfide semiconductor for drastically enhanced visible-light photocatalytic hydrogen evolution. *Appl. Catal. B Environ.* **2018**, *238*, 27–37. [CrossRef]
45. Li, N.; Zhang, Y.; Jia, M.; Lv, X.; Li, X.; Li, R.; Ding, X.; Zheng, Y.Z.; Tao, X. 1T/2H $MoSe_2$-on-MXene heterostructure as bifunctional electrocatalyst for efficient overall water splitting. *Electrochim. Acta* **2019**, *326*, 134976. [CrossRef]
46. Zhang, L.; Sun, L.; Huang, Y.; Sun, Y.; Hu, T.; Xu, K.; Ma, F. Hydrothermal synthesis of N-doped RGO/$MoSe_2$ composites and enhanced electro-catalytic hydrogen evolution. *J. Mater. Sci.* **2017**, *52*, 13561–13571. [CrossRef]
47. Vikraman, D.; Hussain, S.; Prasanna, K.; Karuppasamy, K.; Jung, J.; Kim, H.S. Facile method to synthesis hybrid phase 1T@2H $MoSe_2$ nanostructures for rechargeable lithium ion batteries. *J. Electroanal. Chem.* **2019**, *833*, 333–339. [CrossRef]
48. Mao, Z.; Wang, C.; Lu, H.; Tang, K.; Li, Q.; Yan, C.; Wang, X. Boron-modified electron transfer in metallic 1T $MoSe_2$ for enhanced inherent activity on per-catalytic site toward hydrogen evolution. *Adv. Mater. Interfaces* **2020**, *7*, 1901560. [CrossRef]
49. Maity, S.; Das, B.; Samanta, M.; Das, B.K.; Ghosh, S.; Chattopadhyay, K.K. $MoSe_2$-amorphous CNT hierarchical hybrid core–shell structure for efficient hydrogen evolution reaction. *ACS Appl. Energ. Mater.* **2020**, *3*, 5067–5076. [CrossRef]
50. Ren, X.; Yao, Y.; Ren, P.; Wang, Y.; Peng, Y. Facile sol-gel synthesis of C@$MoSe_2$ coreshell composites as advanced hydrogen evolution reaction catalyst. *Mater. Lett.* **2019**, *238*, 286–289. [CrossRef]
51. Shi, Y.; Gao, W.; Lu, H.; Huang, Y.; Zuo, L.; Fan, W.; Liu, T. Carbon-nanotube-incorporated graphene scroll-sheet conjoined aerogels for efficient hydrogen evolution reaction. *ACS Sustain. Chem. Eng.* **2017**, *5*, 6994–7002. [CrossRef]